Inorganic Chemistry

Article

pubs.acs.org/IC

Surfactant-Thermal Syntheses, Structures, and Magnetic Properties of Mn–Ge–Sulfides/Selenides

Guodong Zhang,[†] Peizhou Li,[‡] Junfeng Ding,[§] Yi Liu,[⊥] Wei-Wei Xiong,[†] Lina Nie,[†] Tom Wu,[§] Yanli Zhao,[‡] Alfred Iing Yoong Tok,[†] and Qichun Zhang*[,†]

[†]School of Materials Science and Engineering, Nanyang Technological University, Singapore 639798, Singapore

[‡]Division of Chemistry and Biological Chemistry, School of Physical and Mathematical Sciences, Nanyang Technological University, Singapore 637371, Singapore

[§]Physical Sciences and Engineering Division, Solar and Photovoltaics Engineering Research Center, King Abdullah University of Science and Technology, Thuwal 23955-6900, Saudi Arabia

[⊥]Department of Materials Science and Engineering, Zhejiang University, Hangzhou 310027, P. R. China

Supporting Information

ABSTRACT: Although either surfactants or amines have been investigated to direct the crystal growth of metal chalcogenides, the synergic effect of organic amines and surfactants to control the crystal growth has not been explored. In this report, several organic bases (hydrazine monohydrate, ethylenediamine (*en*), 1,2-propanediamine (1,2-*dap*), and 1,3-propanediamine (1,3-*dap*)) have been employed as structure-directing agents (SDAs) to prepare four novel chalcogenides $(Mn_3Ge_2S_7(NH_3)_4$ (**1**), $[Mn(en)_2(H_2O)][Mn(en)_2MnGe_3Se_9]$ (**2**), $(1,2\text{-dapH})_2\{[Mn(1,2\text{-dap})_2]Ge_2Se_7\}$ (**3**), and (1,3-dapH)(puH)$MnGeSe_4$(**4**) (pu = propyleneurea) under surfactant media (PEG-400). These as-prepared new crystalline materials provide diverse metal coordination geometries, including MnS_3N tetrahedra, $MnGe_2Se_7$ trimer, and $MnGe_3Se_{10}$ T2 cluster. Compounds **1**–**3** have been fully characterized by single-crystal X-ray diffraction (XRD), powder XRD, UV–vis spectra, Fourier transform infrared spectroscopy, and thermogravimetric analysis. Moreover, magnetic measurements for compound **1** showed an obvious antiferromagnetic transition at ∼9 K. Our research not only enriches the structural chemistry of the transitional-metal/14/16 chalcogenides but also allows us to better understand the synergic effect of organic amines and surfactants on the crystallization of metal chalcogenides.

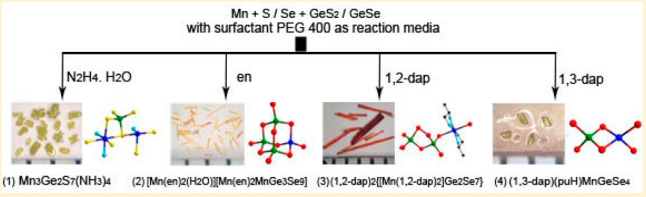

INTRODUCTION

New crystalline metal chalcogenides are very important in materials science because crystalline chalcogenides not only possess diverse structures but also have many potential applications including photocatalysts,[1] field-effect transistors,[2] nonlinear optics,[3] ion exchange,[4] X-ray or γ-ray detections,[5] thermoelectric,[6] topological insulators,[7] Li^+ superionic conductors,[8] and magnetism.[9] Generally, crystalline chalcogenides can be prepared through high-temperature solid-state reactions, flux synthesis, hydro(solvo)thermal methods, and room temperature self-assembly processes. Among them, hydro(solvo)thermal synthesis represents a milder and softer synthetic technique with the merits of both kinetic and thermodynamic control during the reaction process.[10] Consequently, numerous crystalline ternary or quaternary chalcogenides with diverse structures and unique properties have been prepared through the hydro(solvo)thermal method.[10] More recently, ionic liquids[11] have been demonstrated as a new type of reaction media for synthesizing novel inorganic materials including zeolites,[12] metal organic frameworks,[13] oxides,[14] and chalcogenides.[3a,15] However, the price and poor commercially available sources have limited their further exploration as reaction media. Given the disadvantages of ionic liquids, our group recently developed a new strategy (surfactant-thermal method) to prepare crystalline metal chalcogenides and metal organic frameworks (MOFs)[16] because surfactants are much cheaper and can have multifunctional properties such as acidic, basic, neutral, cationic, anionic, or even block. Our further research demonstrated that the syntheses through surfactant media not only can provide novel crystalline chalcogenides/MOFs with diverse structures[16] but also can kinetically control the formation of intermediate phases during the reaction.[17] Nevertheless, such applications in chalcogenide chemistry is still at an early stage, and the effect of surfactants on the growth of chalcogenides is still not very clear. On the other hand, amines have been widely demonstrated as structure-directing agents (SDAs) to control the growth of crystalline inorganic materials due to their different physical properties and various roles during the crystal growth or in the final products.[10h] Thus, it is highly desirable to introduce amines into surfactant-thermal

Received: June 2, 2014
Published: September 10, 2014

dx.doi.org/10.1021/ic501282d | *Inorg. Chem.* 2014, 53, 10248–10256

Table 1. Crystallographic Data and Structure Refinements for Compounds 1−4

chemical formula	$N_4H_{12}Mn_3Ge_2S_7$ (1)	$C_8N_8OH_{34}Mn_3Ge_3Se_9$ (2)	$C_{12}N_8H_{42}MnGe_2Se_7$ (3)	$C_7N_4OH_{20}MnGeSe_4$ (4)
formula weight	602.56	1351.70	1051.38	619.64
space group	*Pbcn* (60)	$P2_1/m$ (11)	*C*2/*c* (15)	$P\bar{1}$ (2)
a (Å)	9.1068 (2)	7.6046 (2)	16.4989(2)	6.4841(8)
b (Å)	13.923 (3)	19.8371 (7)	14.3730(2)	9.3282(1)
c (Å)	12.750 (3)	10.7692 (4)	13.3276(2)	14.586(2)
α (deg)	90.00	90.00	90.00	85.438(5)
β (deg)	90.00	94.893 (3)	92.6110(10)	86.152(4)
γ (deg)	90.00	90.00	90.00	75.290(4)
V (Å^3)	1616.6 (6)	1618.65 (9)	3157.21(8)	849.6(2)
Z	4	2	4	2
D_{cal} (g/cm^3)	2.690	2.747	2.948	2.400
theta (deg)	3.1−27.5	3.2−27.5	4.08−73.08	2.26−29.47
GOF on F^2	1.120	1.026	1.066	1.066
R_1,[a] wR_2[b] [$I > 2\sigma(I)$]	0.0247, 0.0517	0.0465, 0.0571	0.0445, 0.1293	0.0550, 0.0871
R_1, wR_2 (all data)	0.0282, 0.0528	0.1265, 0.1336	0.0466, 0.1317	0.1334, 0.1639

[a] $R_1 = \sum||F_o| - |F_c||/\sum|F_o|$. [b] $wR_2 = [\sum w(F_o^2 - F_c^2)^2]/\sum w(F_o^2)^2]^{1/2}$.

conditions and investigate the synergic effect of organic amines and surfactants on the crystallization of metal chalcogenides.

Following our pioneering works to prepare crystalline thioarsenates and selenidostannates under surfactant-thermal conditions,[16a] we are interested in understanding how different amines to control the crystal growth in Mn−Ge-sulfides/selenide system under surfactant-thermal conditions. In this report, four different crystalline Mn−Ge-sulfides/selenides, namely, $Mn_3Ge_2S_7(NH_3)_4$ (**1**), $[Mn(en)_2(H_2O)][Mn(en)_2$-$MnGe_3Se_9]$ (**2**), $(1,2\text{-dapH})_2\{[Mn(1,2\text{-dap})_2]Ge_2Se_7\}$ (**3**), and (1,3-dapH)(*puH*)$MnGeSe_4$ (**4**) (*en* = ethylenediamine; *1,2-dap* = 1,2-propanediamine; *1,3-dap* = 1,3-propanediamine; *pu* = propyleneurea) have been successfully prepared and fully characterized. Our research could provide us a better understanding of the effects of different amines on the crystallizations and the constructions of Mn−Ge-sulfides/selenides under surfactant-thermal conditions.

EXPERIMENTAL SECTION

Materials Information. The precursors GeS_2 and GeSe were synthesized through a solid state reaction method. Sulfur and selenium were purchased from Alfa Aesar Company. Hydrazine monohydrate, PEG-400, ethylenediamine (*en*), 1,2-propanediamine (*1,2-dap*), and 1,3-propanediamine (*1,3-dap*) were obtained from Sigma-Aldrich Company. Mn was bought from Merck Company. All chemicals were used as received without further purification.

Syntheses. To synthesize compound **1**, Mn (1.0 mmol, 0.055 g), GeS_2 (0.5 mmol, 0.068 g), S (2.5 mmol, 0.080 g), hydrazine monohydrate (0.4 mL, 98%), and PEG-400 (1 g) were mixed together and sealed in a stainless steel autoclave with a 23 mL Teflon-liner. (***Note****: Much attention should be paid due to hydrazine monohydrate toxicity and strongly reducing ability.*) The autoclave was heated at 160 °C for 5 days and then taken out from the oven and cooled to room temperature naturally. The green block crystals (**1**, $Mn_3Ge_2S_7(NH_3)_4$) were collected by hand, washed with ethanol, and dried in air. The compounds are stable under ambient conditions and insoluble in common solvents.

A similar procedure was employed for the syntheses of compounds **2**−**4**. Typically, GeS_2, S, and hydrazine monohydrate were replaced by GeSe (0.5 mmol, 0.076 g), Se (2.5 mmol, 0.197 g), and the corresponding amines (*en*, *1,2-dap*, or *1,3-dap*) to prepare compounds **2**, **3**, **4**, respectively. Note that compound **4** is not stable in air and its characterization is incomplete.

Elemental analysis (EA) for compounds **1**, Calcd, N: 9.30, H: 2.00; Found, N: 9.15, H: 1.86; compounds **2**, Calcd, C: 7.11, N: 8.29, H: 2.54; Found, C: 7.07, N: 8.35, H: 2.48; and compounds **3**, Calcd, C: 13.71, N: 10.66, H: 4.03; Found, C: 13.58, N: 10.75, H: 3.89. No EA is available for compounds **4** due to its poor stability in air. EDX analyses for compounds **1**−**4** are provided in Supporting Information as Figures S1−S4.

Single-Crystal Structure Determination. Single-crystal X-ray diffraction data of **1**, **2**, and **4** were collected on a Bruker APEX II CCD diffractometer equipped with a graphite-monochromatized Mo Kα (0.71073 Å) radiation source at 293 K. The diffraction data of **3** were collected on a Cu Kα (1.54178 Å) radiation source at 293 K. Since N3 in compound **3** was disordered, it was refined with a split mode. The structure was solved by direct methods and refined by full-matrix least-squares on F^2 using the SHELX-97 program package.[18] All of the non-hydrogen atoms were refined with anisotropic thermal parameters. Crystallographic data and structural refinements are summarized in Table 1.

Characterization. Except compound **4** (not stable in the air), the characterizations and property studies of all other three samples **1**−**3** were completely carried out. X-ray powder diffractions were recorded on a Bruker D8 Advance diffractometer with a graphite-monochromatized Cu K_α radiation with the operating angle 2θ ranging from 5° to 65°. The UV−vis absorption spectra were obtained at room temperature on a model UV-2501 PC using $BaSO_4$ plates as standard (100% reflectance). The absorption (α/S) data were calculated from the reflectance using the Kubelka−Munk function: $\alpha/S = (1 - R)^2/2R$, in which, α is the absorption coefficient, R is the reflectance, and S is the scattering wavelength. The band gap values were obtained by extrapolating the linear regions of $(\alpha/S)^2$ versus energy plot to $(\alpha/S)^2 = 0$. The FTIR spectra (KBr pellets) were recorded on a PerkinElmer FTIR spectrophotometer in the range 500−4000 cm^{-1}. Thermogravimetric analysis (TGA) scans were performed on a TGA Q500 instrument in a flowing nitrogen atmosphere with a heating rate of 10 °C/min.

Magnetic Susceptibility. The direct current magnetic susceptibilities for compounds **1**−**3** were measured on an MPMS magnetometer at temperature between 5 and 300 K. Magnetic field up to 2 T were used for the isothermal magnetizations at temperature between 5 and 300 K. All samples were grounded to fine powders in order to minimize possible anisotropic effects and were loaded into a gelatin capsule. A constant magnetic field of 5000 Oe was applied for the measurements of magnetization versus temperature. The data were corrected for the susceptibility of the container and for the diamagnetic contribution from the ion core.

RESULTS AND DISCUSSION

Synthesis. Four novel crystals in Mn−Ge−S/Se system have been synthesized by employing different amines as SDAs under surfactant-thermal conditions (PGE-400 as a surfactant).

dx.doi.org/10.1021/ic501282d | *Inorg. Chem.* 2014, 53, 10248−10256

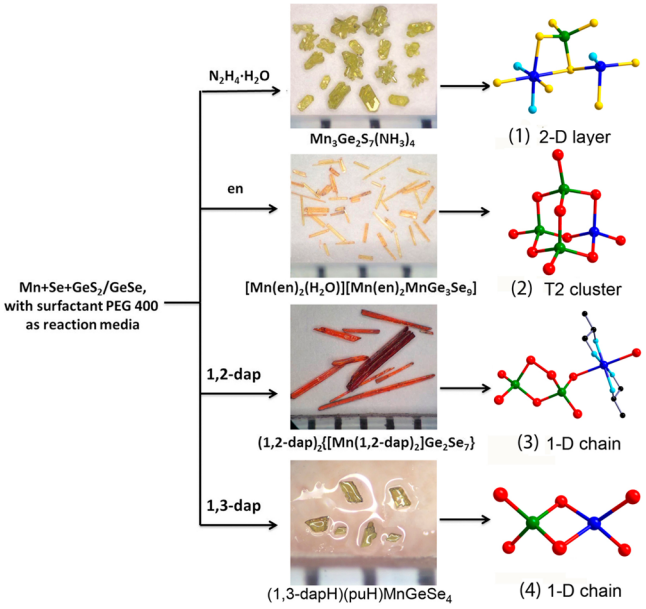

Figure 1. Reaction routes, photographs, and the typical coordination environments of Mn and Ge in compounds **1**−**4**. All of the reactions were conducted under solvothermal conditions in PEG-400. The Mn, Ge, S, Se, C, and N atoms are drawn as blue, green, yellow, red, black, and skyblue balls.

Figure 1 summarized the reaction conditions, photographs of corresponding crystals, and the typical structure features of compounds **1**−**4**. Using hydrazine monohydrate as an SDA, compound **1** was obtained as green block crystals in 58% yield (based on Mn), which are stable in the ambient environment for several months. Using *en* as a direction agent, compound **2** was harvested as yellow rod-like crystals in ∼43% yield (based on Mn). Although an analogue (sulfide-based) of compound **2** has been reported by Wang's group,[19] they failed in preparing selenium-based complexes under the same condition. In our research, we found that PEG-400 plays an important role in preparing compound **2**, and no crystals were obtained if PEG-400 was removed from reaction system. When *en* was replaced by *1,2-dap* and *1,3-dap*, rod-like red crystals **3** and green block crystals **4** were obtained in the yields of ∼22% and ∼30% (based on Mn), respectively. Note that compound **4** is sensitive to air and moisture and it would change its color to brown after exposure in air for several hours. The existence of Mn, Ge, S/Se for compounds **1**−**4** were further confirmed by the elemental analyses based on an EDX-equipped JEOL/JSM-6360A SEM (see EDX results in Figures S1−S4, Supporting Information).

It is well-known that the structure factors of chalcogenides are very sensitive to synthetic conditions including reaction media, pH, temperature, and reaction time. Among them, the reaction media plays an essential role in promoting the crystallization of chalcogenides. To investigate the effect of PEG-400 on the formation of crystalline Mn−Ge-chalcogenides, a series of reactions were carried out in conventional solvents such as water, ethylene glycol, methanol, and hydrazine (see Table S1, Supporting Information). These results clearly show that no crystals can be formed if PEG-400 was removed from reaction systems, which suggests that the surfactant is very important to help the crystal growth. Although the effects of surfactants on the crystallization are still not well-understood, the coordination ability, viscidity, and

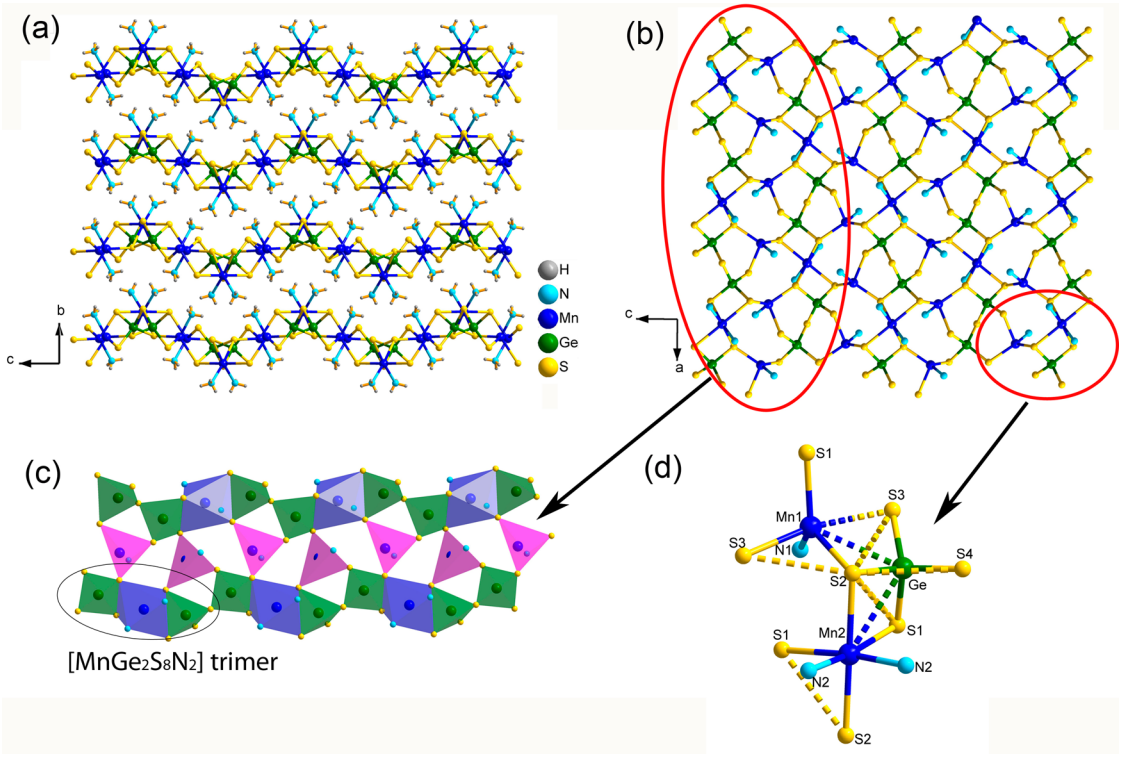

Figure 2. (a) View of two-dimensional frameworks of compound **1** down the *a*-axis. (b) View of a single layer down the *b*-axis. (c) Polyhedral view of $[MnGe_2S_8N_2]_n$ chains connected by MnS_3N tetrahedra. (d) Complex weak interactions in one layer of compound **1**. The lengths of secondary bonds are as follows: Mn1−S3, 2.866(1) Å; Ge−Mn1, 3.231(1) Å; Ge−Mn2, 3.333(1) Å; S1−S2, 3.496(1) Å; S2−S3, 3.516(1) Å; S2−S3′, 3.575(1) Å; S2−S4, 3.543(1) Å. For clarity, the hydrogen atoms are removed in (b), (c), and (d).

dx.doi.org/10.1021/ic501282d | *Inorg. Chem.* 2014, 53, 10248−10256

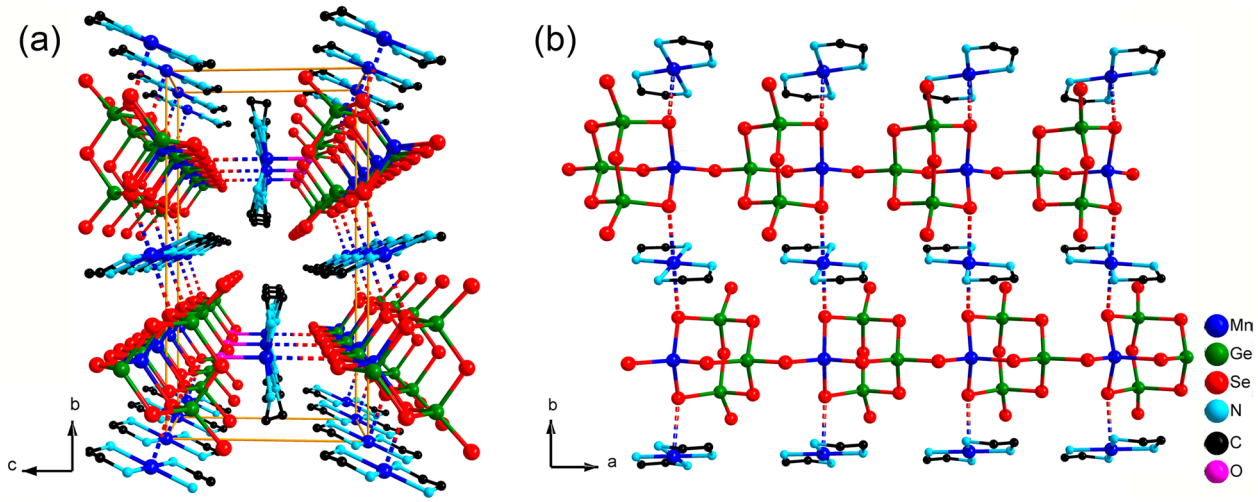

Figure 3. (a) View of compound **2** along the *a*-axis. (b) T2 cluster chains further stack into a quasi-layer structure through Mn−Se secondary bonds (3.006(5) Å) in compound **2**.

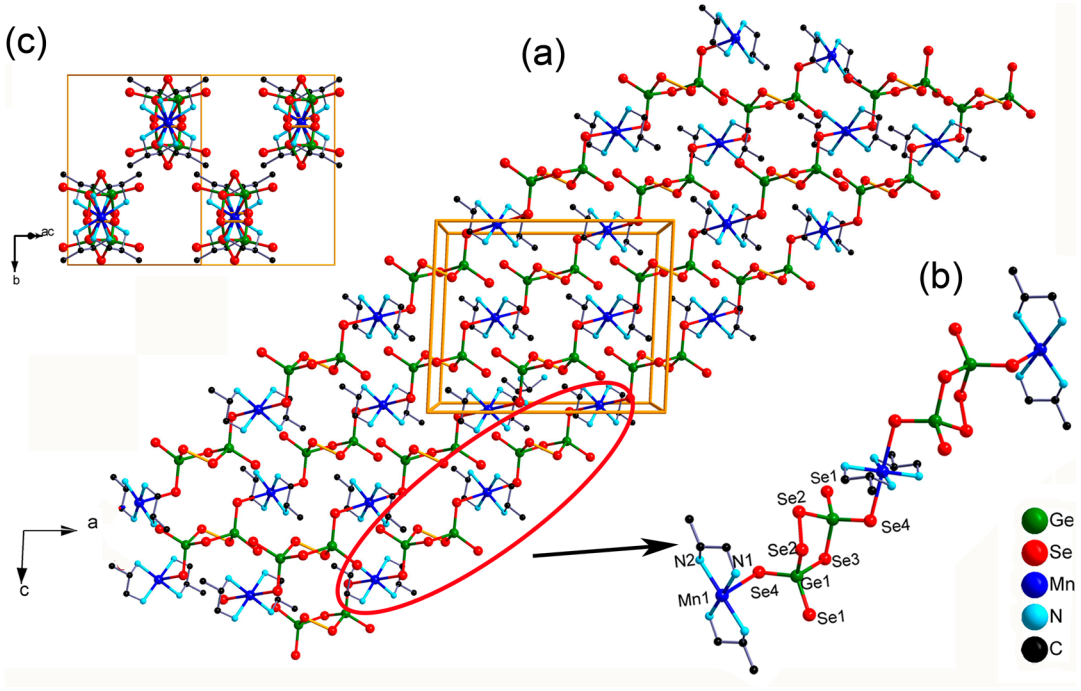

Figure 4. (a) View of compound **3** along the *b*-axis. (b) Isolated $[Mn(1,2\text{-dap})_2]Ge_2Se_7]$ chain in the structure of **3** with the atom numbering scheme. (c) View of compound **3** along the $\langle 10\bar{1} \rangle$ axis. Charge compensating species protonated 1,2-daps in the channels between the chains omitted for clarity in (a) and (c).

Janus characteristics of PEG-400 are believed to have a strong contribution to the solubility and mass transfer of metal ions and organic ligands, thus promoting the crystallization of manganese chalcogenidogermanate system.

Moreover, crystallizations and structural factors of metal chalcogenides are highly dependent on the amines. In this research, the usage of different amines can result in diverse metal coordination geometries and connecting modes including MnS_4N_2 octahedra, MnS_3N tetrahedra, $MnSe_2N_4$ octahedra, $MnSe_4$ tetrahedra, Ge_2Se_7 dimer, and T2 cluster constructed by $MnSe_4$ and $GeSe_4$ tetrahedra. Although hydrazine possesses strong reducing properties, both hydrazine and organic amines show a basic nature, which is very important for the synthesis of chalcogenides. At this point, it is reasonable to discuss them together. In compound **1**, N_2H_4 has been investigated to decompose into NH_3 under surfactant-thermal conditions. In fact, the decomposition of N_2H_4 is a complicated process. In the literature, N_2H_4 can be converted into NH_3 either by O_2/sulfur[20] or with transition metal as catalysis,[21] which might be reduction or oxidation mechanism. Since our reaction contains sulfur, transition metal, and O_2, it is very difficult to confirm that the conversion of N_2H_4 into NH_3 is a reduction process or oxidation process. In addition, our reaction was performed in sealed system under mild temperatures with medium pressure, and it is very difficult for us to obtain enough evidence to support which mechanism is correct. But the as-formed NH_3 was confirmed by single-crystal structure analysis, TGA analysis, and elemental analysis.

dx.doi.org/10.1021/ic501282d | *Inorg. Chem.* 2014, 53, 10248−10256

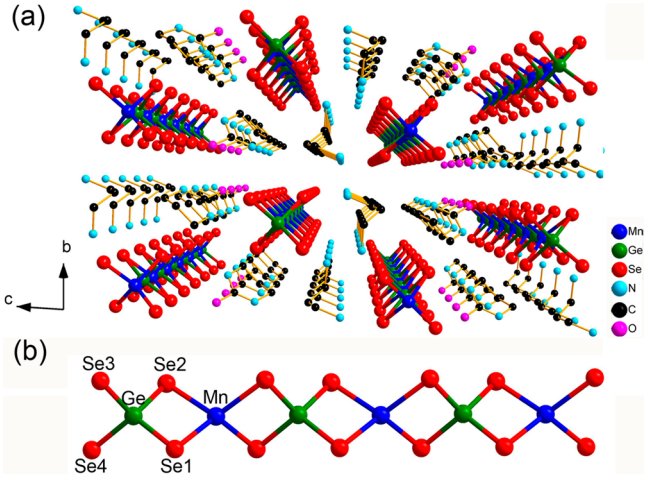

Figure 5. (a) View of compound **4** along the *a*-axis. (b) One chain in the structure of **4** with the atom numbering scheme.

Crystal Structures. $Mn_3Ge_2S_7(NH_3)_4$ (1). As shown in Figure 2a,b, compound **1** crystallizes in orthorhombic space group *Pbcn* (No. 60) and features a two-dimensional network paralleled to the *ac* plane. The asymmetric unit of **1** contains two crystallographically independent Mn atoms, one Ge atom, four S atoms, and two NH_3 neutral molecules (decomposed from N_2H_4). Ge atoms adopt a normally GeS_4 tetrahedral geometry, while Mn centers have two different types of coordination modes: One Mn atom (Mn2) adopts an octahedral geometry MnS_4N_2[9a,22,23] and the other Mn atom (Mn1) has a MnS_3N tetrahedral configuration.[24] In addition, S atoms adopt two coordination geometries: S1 and S2 adopt 3-fold coordination while S3 and S4 possess 2-fold coordination. In the layer (Figure 2c), two GeS_4 tetrahedra coordinate with one MnS_4N_2 octahedra by sharing two S···S edges to form a $[MnGe_2S_8N_2]$ trimer, which further connects each other through sharing one terminal S atom to build a chain along the *a*-axis direction. The two adjacent chains are further linked together by MnS_3N tetrahedra via sharing S1, S2, and S3 atoms to form a two-dimensional network (Figure S5b, Supporting Information). In addition, the complicated weak interactions in the structure of **1** have been shown in Figure 2d and Figure S5a, Supporting Information. These weak interactions together with the weak N−H···S hydrogen bonds are helpful for the stabilization and the stacking of the layers. The distances of Mn−S (2.464(1)−2.547(1) Å) and Mn1−N1 (2.176(3) Å) in MnS_3N unit are slightly shorter than those in MnS_4N_2 species (2.679(1)−2.694(1) Å for Mn−S and 2.219(4) Å for Mn−N).

In the previously reported chalcogenides, hydrazine is often used as an integral part of the framework,[9a,22,23,25] or as guest molecules inside the framework.[26] Recently, we found that the N−N bonds of the hydrazine could be broken under surfactant-thermal conditions.[16a,22] The resulting NH_3 molecules could coordinate with Mn atoms directly. In fact, a similar coordination for the Mn atom was also found in our recently reported compound $[Mn(NH_3)_6][Mn_2As_2S_8(N_2H_4)_2]$,[16a] in which Mn**2** also directly connected with six NH_3 molecules.

$[Mn(en)_2(H_2O)][Mn(en)_2MnGe_3Se_9]$ (2). Compound **2** crystallizes in the monoclinic space group $P2_1/m$ (No. 11) with a quasi-layered structure. As shown in Figure 3b, T2 cluster $[MnGe_3Se_{10}]^{6-}$, similar to $[Ge_4Se_{10}]^{4-}$,[27] is constructed

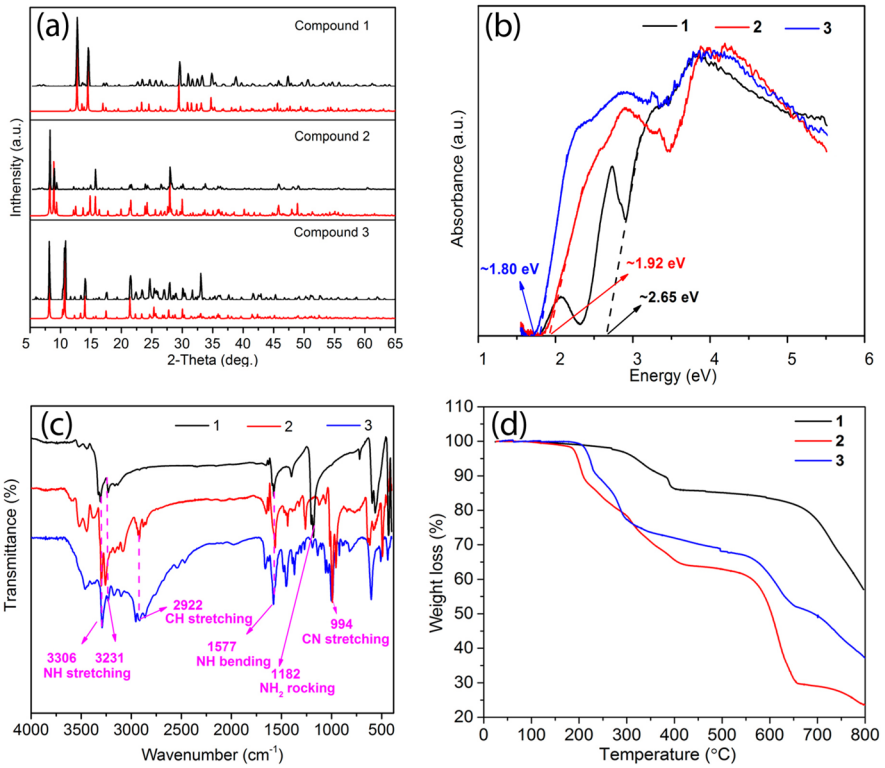

Figure 6. (a) Powder XRD patterns for compounds **1**−**3**. The black lines are the experimental results, and the red lines are the simulated results from single crystals structure. (b) Solid-state UV−vis optical absorption spectra of compounds **1**−**3** with the assignment of optical absorption edges. (c) FTIR spectra for compounds **1**−**3** with the assignment of main absorption peaks. (d) TGA curves for compounds **1**−**3**. N_2 atmosphere, heating rate 10 °C/min.

dx.doi.org/10.1021/ic501282d | *Inorg. Chem.* 2014, 53, 10248−10256

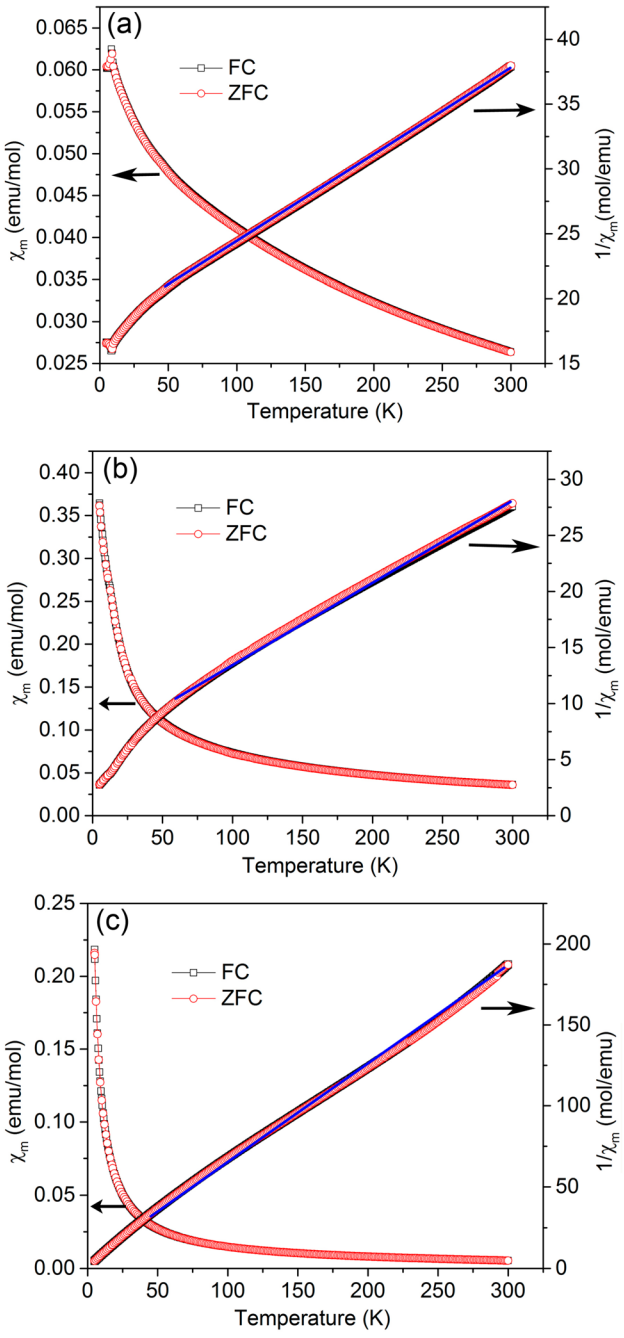

Figure 7. Zero-field-cooled (ZFC) and field-cooled (FC) magnetic susceptibility (χ) and inverse susceptibility (χ^{-1}) between 5 and 300 K for (a) compound **1**, (b) compound **2**, and (c) compound **3**. A linear fitting (blue line) between 50 and 300 K can be performed based on the inverse ZFC susceptibility versus temperature with the Curie–Weiss law.

Table 2. Calculated Magnetic Parameters of Compounds 1–3

	compound **1**	compound **2**	compound **3**
C (emu K/mol)	14.86(7)	13.92(3)	1.722(5)
θ (K)	−260.99(3)	−88.84(1)	−15.20(1)
μ_{eff} (μ_B)	3.63(4)	3.51(7)	3.71(1)

by one $MnSe_4$ tetrahedra and three $GeSe_4$ tetrahedra. The as-resulted T2 clusters further connect each other by sharing terminal Se atoms to form a chain along the *a*-axis. Compound **2** is an isostructural compound with the reported one $[Mn(en)_2(H_2O)][Mn(en)_2MnGe_3S_9]$.[19] The bond lengths of Ge–Se and Mn1–Se in T2 cluster fall in the range of 2.265–2.375 Å and 2.547–2.556 Å, respectively, while the angles Se–Ge–Se and Se–Mn–Se in the same cluster are between 103.441 and 114.792° and between 95.702 and 112.575°, respectively.

$(1,2\text{-dapH})_2\{[Mn(1,2\text{-dap})_2]Ge_2Se_7\}$ (3). Compound **3** possesses the space group $C2/c$ (No. 15) and features a sinusoidal chain along $\langle 10\bar{1}\rangle$ directions (Figure 4a). As shown in Figure 4b, the chain consists of two building units: dimeric $[Ge_2Se_7]^{4-}$ and $[Mn(1,2\text{-dap})_2]^{2+}$. The Ge atom coordinates with four Se atoms to form a tetrahedral configuration, which further forms a $[Ge_2Se_7]^{4-}$ dimer through a Se–Se bond. The dinuclear $[Ge_2Se_7]^{4-}$ further links with two Mn atoms through the terminal two Se atoms to form a one-dimensional infinite chain $[MnGe_2Se_7^{2-}]_n$, which is unknown for a ternary selenidogermanate. Interestingly, 1,2-daps in compound **3** have two roles: as a ligand to combine with Mn atoms to form $[Mn(1,2\text{-dap})_2]^{2+}$ cations and as a counterion after protonation (Figure 4c). The isolated Se2–Se2 bond with the bond length of 2.3365(12) Å is shown in Figure 4b. Note that the bond lengths of $Ge–Se2_{bridge}$ (2.404 Å) and $Ge–Se3_{bridge}$ (2.401 Å) are a little bit longer than those of $Ge–Se1_{terminal}$ (2.283 Å) and $Ge–Se4_{terminal}$ (2.310 Å) as found in previous reports of compounds $(enH_2)[\{Mn(en)_2(enH)\}_2(\mu\text{-en})](Ge_2Se_7)_2$,[28] $[Mn(dien)_2]_2Ge_2Se_7$,[28] and $[\{Mn(cyclam)\}_2(\mu\text{-}Ge_2Se_7)]\cdot CH_3OH\cdot 1.5H_2O$.[29] The length of Mn–Se4 bond (2.858 Å) in compound **3** is much longer than its normal length of 2.5–2.6 Å.[27b]

$(1,3\text{-dapH})(puH)MnGeSe_4$ (4). As shown in Figure 5a, compound **4** crystallizes in triclinic space group $P\bar{1}$ (No. 2) and features a one-dimensional structure along the *a*-axis. The chain is made up of anionic $[MnGeSe_6]^{2-}$ dimers through sharing their edges (Figure 5b). The bond lengths of Ge–Se and Mn–Se are in the range of 2.348–2.363 Å, and 2.550–2.571 Å, respectively.[30] Although similar anionic chains $[MM'Q]_6^{2-}$ (M = Mn, Hg, Zn; M′ = Ge, Sn; Q = S, Se, Te) have been reported in several compounds such as $A_2[MSnQ_4]$ (A = K, Et_4N, Me_4N; M = Mn, Hg; Q = Se, Te),[31] $[1,4\text{-dabH}]_2[MnSnS_4]$ (1,4-dabH = 1,4-diaminobutane),[32] $[AEP][PPZH]_3[Zn_2Ge_2Se_8]$ (AEP = *N*-(2-aminoethyl)piperazine, PPZ = piperazine),[33] and $[DBNH][M_{1/2}Sn_{1/2}Se_2]$ (M = Mn, Hg, Zn),[34] compound **4** is the first example of anionic chain structure for thiogermanate integrated with Mn^{2+} ions.

Additionally, two types of organic cations coreside as counterions between the chains. One is the protonated 1,3-diaminopropane cation and the other is the protonated propyleneurea cation formed through the reaction of 1,3-diaminopropane with CO_2 in PEG-400.[35] A similar phenomenon was also observed in other solvothermal reactions.[35]

Characterizations. The powder X-ray diffraction patterns of **1**–**3** are matched very well with the corresponding simulated results from the single-crystal diffraction data (Figure 6a), which indicates the pure phases for all as-obtained samples. The solid state UV–visible absorption spectra of **1**–**3** are shown in Figure 6b. The bandgaps for **1**, **2**, and **3** are ∼2.65 eV, ∼1.92 eV, and ∼1.80 eV, respectively, which are in accordance with their green color, orange-yellow color, and orange-red color. Additionally, the absorption below the band gap transition at about 2.1 eV for compound **1** is attributed to midgap states associated with Mn-based d–d transitions,[36] which are also

dx.doi.org/10.1021/ic501282d | *Inorg. Chem.* 2014, 53, 10248–10256

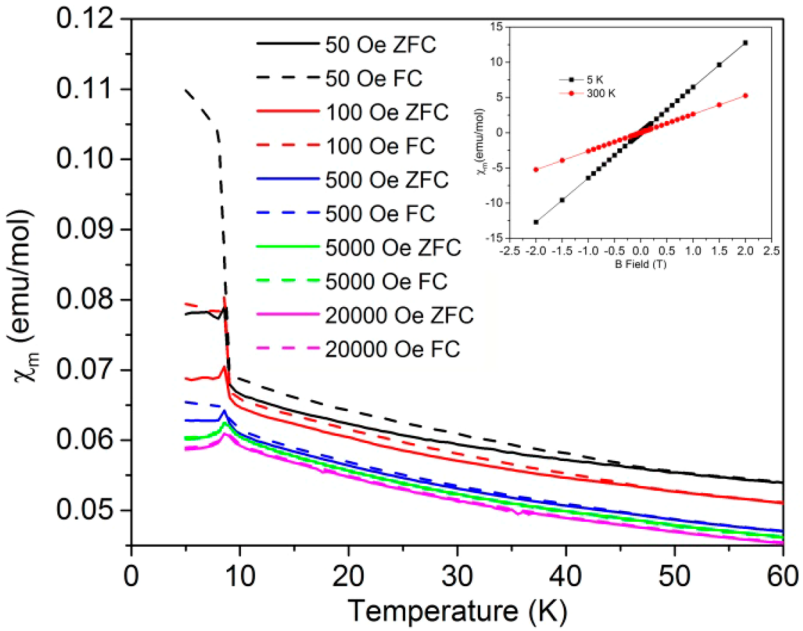

Figure 8. Zero-field-cooled (ZFC) and field-cooled (FC) magnetic susceptibility (χ) of compound **1** as a function of temperature at different applied fields. Inset is the magnetic susceptibility versus magnetic field B at 5 and 300 K.

observed in other compounds such as $Mn_2SnS_4(N_2H_4)_2$,[9a] $[Mn(en)_2(H_2O)][Mn(en)_2MnGe_3S_9]$,[19] and $[Mn(en)_2]_2Sn_2S_6$.[19]

FTIR spectra of **1**−**3** are provided in Figure 6c. For compound **1**, the peaks between 1204 and 1182 cm^{-1} can be assigned to the NH_2 rocking.[22] Note that any vibration peaks at 940 and 960 cm^{-1} (vibration peaks of N−N bonds) in compound **1** are investigated, confirming that there is no existence of N_2H_4 in this complex,[9a] which is in agreement with the result from the structure analysis of single crystal X-ray crystallography. The peaks between 3308 and 3231 cm^{-1} and at the position of about 1577 cm^{-1} belong to N−H stretching and N−H bond bending, respectively. In addition, the strong peak at about 994 cm^{-1} can be assigned to the stretching vibrations of C−N bonds.

The thermogravimetric analysis (TGA) results for compounds **1**−**3** are shown in Figure 6d. For compound **1**, there is nearly no weight loss up to 300 °C. A significant weight loss (∼13.7%) was observed between 300 and 450 °C, which is close to the complete removal of NH_3 molecules in the compound **1** (11.3%). Compound **2** starts to lose its weight at 180 °C, and the total weight loss between 180 and 540 °C is about 38.4%, which might contribute from the loss of *en* ligands, H_2O and Se. Compound **3** could be stable up to 200 °C, and the weight loss (∼7.8%) between 200 and 250 °C is close to the calculated amount (7.6%) of free organic 1,2-dap molecules in this compound, while the weight loss (16.5%) between 250 and 300 °C could contribute from two coordinated 1,2-dap (15.2%) molecules. The progressive weight loss above 680 °C for **1** and 550 °C for **2** and **3** could be explained by the continuous decomposition and sublimation of S or Se at elevated temperature.

Magnetism. Zero-field-cooled (ZFC) and field-cooled (FC) magnetic susceptibility data for compounds **1**−**3** are shown in Figure 7. For **1** and **2**, the $1/\chi_m$ vs T curves below 50 K significantly deviates from linearity. For compound **1**, an obvious peak (centered at ∼9 K) in the plot of susceptibility vs temperature is observed, indicating an antiferromagnetic ordering of Mn^{2+} ions. The data for all three compounds were fitted by the Curie−Weiss law in the temperature range of 50−300 K, using the following equation

$$\chi = \frac{C}{T - \theta}$$

where C and θ mean the Curie constant and Weiss constant, respectively. The effective magnetic moment (μ_{eff}) was calculated from the equation $\mu_{eff} = (7.997 \times C)^{1/2}\ \mu_B$. The magnetic parameters for compounds **1**−**3** were calculated based on the data from the plot of magnetic susceptibility vs temperature and have been summarized in Table 2. The large negative Weiss constant for compound **1** (−260.99 K) indicates that a considerably strong antiferromagnetic (AF) couple dominates the exchange among magnetic Mn ions.

For compound **1**, the magnetic susceptibilities were measured as a function of the temperature at different applied fields. As shown in Figure 8, the data at low applied fields (50, 100, or 500 Oe) became deviation between ZFC and FC data below about 44 K, which becomes less pronounced above 500 Oe (5000 Oe, and 20000 Oe). This result implies that there is another transition at about 44 K besides the antiferromagnetic transition at 9 K. However, no hysteretic phenomenon was observed in M−H curves even measured at 5 K. Considering that there are two crystallographically independent Mn^{2+} dites, i.e., MnS_4N_2 octahedral geometry and MnS_3N tetrahedral geometry, we presume that the disappearance of hysteresis loop at 5 K is attributed to the coexistence of ferromagnetic phase and paramagnetic phase, i.e., only part of Mn^{2+} moments in compound **1** ferromagnetically aligned. This result is similar to the reported results in compounds $Mn_2SnS_4(N_2H_4)_2$,[9a] $Mn_2Sb_2S_5(N_2H_4)_3$,[22] and $Mn_2Sb_4S_8(N_2H_4)_2$.[23] Although the amount of AFM phase (in MnS_4N_2 octahedral geometry) is two times larger than that of the ferromagnetic phase (in MnS_2N tetrahedral geometry), compound **1** still shows a paramagnetic behavior. In addition, the formation of the ferromagnetic phase might also explain the decrease of μ_{eff}

dx.doi.org/10.1021/ic501282d | Inorg. Chem. 2014, 53, 10248−10256

(3.63 μ_B), which is lower than the spin-only value expected for the Mn^{2+} ($3d^5$) ion in a high-spin state (5.92 μB).

CONCLUSIONS

In this report, the effect of different amines on the construction of manganese chalcogenidogermanate under surfactant (PEG-400)-thermal condition has been investigated. Four novel crystals $Mn_3Ge_2S_7(NH_3)_4$ (**1**), $[Mn(en)_2(H_2O)][Mn(en)_2MnGe_3Se_9]$ (**2**), $(1,2\text{-dapH})_2\{[Mn(1,2\text{-dap})_2]Ge_2Se_7\}$ (**3**), and (1,3-dapH)(puH)$MnGeSe_4$ (**4**) have been successfully prepared in similar reaction conditions by choosing different bases (*hydrazine, en, 1,2-dap, and 1,3-dap*) as SDAs. Compound **1** processes a two-dimensional layer structure, while compound **2** has chainlike structures constructed from $[MnGe_3Se_{10}]^{6-}$ T2 clusters. Compound **3** features a one-dimensional chain made from $[Ge_2Se_7]^{4-}$ dimers and $[Mn(1,2\text{-dap})_2]^{2+}$ species, and compound **4** is one-dimensional polymer made from $[MnGeSe_6]^{2-}$ clusters. The purity, band gap, and thermal stability for compounds **1**−**3** have been fully characterized by powder XRD, UV−vis spectra, FTIR spectroscopy, and thermogravimetric analysis. Furthermore, magnetic susceptibility measurements show that compounds **1**−**3** display paramagnetic behaviors near room temperature. However, when the temperature decreases to 9 K, an obvious antiferromagnetic transition in compound **1** can be observed. Our success in demonstrating that amines could direct the crystal growth of chalcogenides under surfactant-thermal condition could provide a new way to prepare crystalline inorganic materials.

ASSOCIATED CONTENT

Supporting Information

The summary of initial compositions and final products in Table S1, crystallographic files in CIF format, atomic parameters (Tables S2−S5), and EDX results (Figures S1−S4) of compounds **1**−**4**. This material is available free of charge via the Internet at http://pubs.acs.org.

AUTHOR INFORMATION

Corresponding Author

*E-mail: qczhang@ntu.edu.sg. Phone: +65-67904705. Fax: +65-67904705.

Notes

The authors declare no competing financial interest.

ACKNOWLEDGMENTS

Q.Z. acknowledges financial support from AcRF Tier 1 (RG 16/12) and Tier 2 (ARC 20/12 and ARC 2/13) from MOE, and the CREATE program (Nanomaterials for Energy and Water Management) from NRF, Singapore.

REFERENCES

(1) (a) Zheng, N.; Bu, X.; Vu, H.; Feng, P. *Angew. Chem., Int. Ed.* **2005**, *44*, 5299−5303. (b) Zhang, Z. Y.; Zhang, J.; Wu, T.; Bu, X. H.; Feng, P. Y. *J. Am. Chem. Soc.* **2008**, *130*, 15238−15239. (c) Zheng, N.; Bu, X.; Feng, P. *Chem. Commun.* **2005**, *22*, 2805−2807.

(2) Milliron, D. J.; Mitzi, D. B.; Copel, M.; Murray, C. E. *Chem. Mater.* **2006**, *18*, 587−590.

(3) (a) Zhang, Q.; Chung, I.; Jang, J. I.; Ketterson, J. B.; Kanatzidis, M. G. *J. Am. Chem. Soc.* **2009**, *131*, 9896−9897. (b) Chung, I.; Kanatzidis, M. G. *Chem. Mater.* **2014**, *26*, 849−869. (c) Yin, W.; Feng, K.; Hao, W.; Yao, J.; Wu, Y. *Inorg. Chem.* **2012**, *51*, 5839−5843. (d) Chen, Y. K.; Chen, M. C.; Zhou, L. J.; Chen, L.; Wu, L. M. *Inorg.Chem.* **2013**, *52*, 8334−8341. (e) Zhang, Q.; Chung, I.; Jang, J. I.; Ketterson, J. B.; Kanatzidis, M. G. *Chem. Mater.* **2009**, *21*, 12−14. (f) Chen, M.-C.; Wu, L. M.; Lin, H.; Zhou, L. J.; Chen, L. *J. Am. Chem. Soc.* **2012**, *134*, 6058−6060. (g) Yu, P.; Zhou, L. J.; Chen, L. *J. Am. Chem. Soc.* **2012**, *134*, 2227−2235.

(4) (a) Zheng, N. F.; Bu, X.; Wang, B.; Feng, P. Y. *Science* **2002**, *298*, 2366−2369. (b) Ding, N.; Kanatzidis, M. G. *Nat. Chem.* **2010**, *2*, 187−191. (c) Wang, K. Y.; Feng, M. L.; Li, J. R.; Huang, X. Y. *J. Mater. Chem. A* **2013**, *1*, 1709−1715. (d) Feng, M. L.; Kong, D. N.; Xie, Z. L.; Huang, X. Y. *Angew. Chem., Int. Ed.* **2008**, *47*, 8623−8626.

(5) (a) Li, H.; Malliakas, C. D.; Liu, Z.; Peters, J. A.; Jin, H.; Morris, C. D.; Zhao, L.; Wessels, B. W.; Freeman, A. J.; Kanatzidis, M. G. *Chem. Mater.* **2012**, *24*, 4434−4441. (b) Li, H.; Malliakas, C. D.; Peters, J. A.; Liu, Z.; Im, J.; Jin, H.; Morris, C. D.; Zhao, L. D.; Wessels, B. W.; Freeman, A. J.; Kanatzidis, M. G. *Chem. Mater.* **2013**, *25*, 2089−2099.

(6) (a) Biswas, K.; He, J. Q.; Zhang, Q.; Wang, G. Y.; Uher, C.; Dravid, V. P.; Kanatzidis, M. G. *Nat. Chem.* **2011**, *3*, 160−166. (b) Ahn, K.; Biswas, K.; He, J.; Chung, I.; Dravid, V.; Kanatzidis, M. G. *Energy Environ. Sci.* **2013**, *6*, 1529−1537. (c) Guin, S. N.; Chatterjee, A.; Negi, D. S.; Datta, R.; Biswas, K. *Energy Environ. Sci.* **2013**, *6*, 2603−2608. (d) Zhao, L. D.; Wu, H. J.; Hao, S. Q.; Wu, C. I.; Zhou, X. Y.; Biswas, K.; He, J. Q.; Hogan, T. P.; Uher, C.; Wolverton, C.; Dravid, V. P.; Kanatzidis, M. G. *Energy Environ. Sci.* **2013**, *6*, 3346−3355. (e) Zhang, Q.; Malliakas, C. D.; Kanatzidis, M. G. *Inorg. Chem.* **2009**, *48*, 10910−10912.

(7) (a) Zhang, H. J.; Liu, C. X.; Qi, X. L.; Dai, X.; Fang, Z.; Zhang, S. C. *Nat. Phys.* **2009**, *5*, 438−442. (b) Zhang, G. H.; Qin, H. J.; Teng, J.; Guo, J. D.; Guo, Q. L.; Dai, X.; Fang, Z.; Wu, K. H. *Appl. Phys. Lett.* **2009**, *95*, 053114. (c) Chen, Y. L.; Analytis, J. G.; Chu, J. H.; Liu, Z. K.; Mo, S. K.; Qi, X. L.; Zhang, H. J.; Lu, D. H.; Dai, X.; Fang, Z.; Zhang, S. C.; Fisher, I. R.; Hussain, Z.; Shen, Z. X. *Science* **2009**, *325*, 178−181. (d) Jin, H. S.; Song, J. H.; Freeman, A. J.; Kanatzidis, M. G. *Phys. Rev. B* **2011**, *83*, 041202. (e) Johnsen, S.; Peter, S. C.; Nguyen, S. L.; Song, J. H.; Jin, H.; Freeman, A. J.; Kanatzidis, M. G. *Chem. Mater.* **2011**, *23*, 4375−4383.

(8) (a) Kamaya, N.; Homma, K.; Yamakawa, Y.; Hirayama, M.; Kanno, R.; Yonemura, M.; Kamiyama, T.; Kato, Y.; Hama, S.; Kawamoto, K.; Mitsui, A. *Nat. Mater.* **2011**, *10*, 682−686. (b) Bron, P.; Johansson, S.; Zick, K.; Schmedtauf der Günne, J.; Dehnen, S.; Roling, B. *J. Am. Chem. Soc.* **2013**, *135*, 15694−15697.

(9) (a) Manos, M. J.; Kanatzidis, M. G. *Inorg. Chem.* **2009**, *48*, 4658−4660. (b) Zhang, Q.; Bu, X.; Lin, Z.; Biasini, M.; Beyermann, W.; Feng, P. *Inorg. Chem.* **2007**, *46*, 7262−7264.

(10) (a) Feng, P. Y.; Bu, X. H.; Zheng, N. F. *Acc. Chem. Res.* **2005**, *38*, 293−303. (b) Dehnen, S.; Melullis, M. *Coord. Chem. Rev.* **2007**, *251*, 1259−1280. (c) Kanatzidis, M. G.; Poeppelmeier, K. R. *Prog. Solid State Chem.* **2008**, *36*, 1−133. (d) Zhang, Q.; Bu, X.; Lin, Z.; Feng, P. *Chem. Mater.* **2008**, *20*, 3239−3241. (e) Zhang, Q.; Armatas, G.; Kanatzidis, M. G. *Inorg. Chem.* **2009**, *48*, 8665−8667. (f) Liu, Y.; Boey, F.; Lao, L. L.; Zhang, H.; Liu, X.; Zhang, Q. *Chem.—Asian J.* **2011**, *6*, 1004−1006. (g) Xiong, W. W.; Zhang, G. D.; Zhang, Q. *Inorg. Chem. Front.* **2014**, *1*, 292−301. (h) Sheldrick, W. S.; Wachhol, M. *Angew. Chem., Int. Ed.* **1997**, *36*, 206−224.

(11) Ma, Z.; Yu, J.; Dai, S. *Adv. Mater.* **2010**, *22*, 261−285.

(12) (a) Lin, Z. J.; Slawin, A. M. Z.; Morris, R. E. *J. Am. Chem. Soc.* **2007**, *129*, 4880. (b) Lin, Z. J.; Wragg, D. S.; Warren, J. E.; Morris, R. E. *J. Am. Chem. Soc.* **2007**, *129*, 10334.

(13) (a) Zhao, Y. J.; Zhang, J. L.; Han, B. X.; Song, J. L.; Li, J. S.; Wang, Q. A. *Angew. Chem., Int. Ed.* **2011**, *50*, 636−639. (b) Fu, H.; Li, Y. G.; Lu, Y.; Chen, W. L.; Wu, Q. O.; Meng, J. X.; Wang, X. L.; Zhang, Z. M.; Wang, E. B. *Cryst. Growth. Des.* **2011**, *11*, 458−465. (c) Freudenmann, D.; Wolf, S.; Wolff, M.; Feldmann, C. *Angew. Chem., Int. Ed.* **2011**, *50*, 11050−11060.

(14) (a) Wang, G.; Valldor, M.; Spielberg, E. T.; Mudring, A.-V. *Inorg. Chem.* **2014**, *53*, 3072−3077. (b) Wang, G. M.; Valldor, M.; Lorbeer, C.; Mudring, A. V. *Eur. J. Inorg. Chem.* **2012**, *2012*, 3032−3038.

(15) (a) Biswas, K.; Zhang, Q.; Chang, I.; Song, J.-H.; Androulakis, J.; Freeman, A.; Kanatzidis, M. G. *J. Am. Chem. Soc.* **2010**, *132*, 14760−14762. (b) Li, J. R.; Xie, Z. L.; He, X. W.; Li, L. H.; Huang, X. Y. *Angew. Chem., Int. Ed.* **2011**, *50*, 11395−11399. (c) Ahmed, E.; Isaeva, A.; Fiedler, A.; Haft, M.; Ruck, M. *Chem.—Eur. J.* . **2011**, *17*, 6847−6852. (d) Lin, Y. M.; Dehnen, S. *Inorg. Chem.* **2011**, *50*, 7913−7915. (e) Lin, Y. M.; Massa, W.; Dehnen, S. *J. Am. Chem. Soc.* **2012**, *134*, 4497−4500.
(16) (a) Xiong, W. W.; Athresh, E. U.; Ng, Y. T.; Ding, J.; Wu, T.; Zhang, Q. *J. Am. Chem. Soc.* **2013**, *135*, 1256−1259. (b) Gao, J.; Ye, K.; Yang, L.; Xiong, W.-W.; Ye, L.; Wang, Y.; Zhang, Q. *Inorg. Chem.* **2014**, *53*, 691−693. (c) Gao, J.; He, M.; Lee, Z. Y.; Cao, W. F.; Xiong, W.-W.; Li, Y.; Ganguly, R.; Wu, T.; Zhang, Q. *Dalton Trans.* **2013**, *42*, 11367−11370. (d) Gao, J.; Ye, K.; He, M.; Cao, W.; Xiong, W.-W.; Lee, Z. Y.; Wang, Y.; Wu, T.; Huo, F.; Liu, X.; Zhang, Q. *J. Solid State Chem.* **2013**, *206*, 27−31. (e) Lu, H.-S.; Bai, L.; Xiong, W.-W.; Li, P.; Ding, J.; Zhang, G.; Wu, T.; Zhao, Y.; Lee, J.; Yang, Y.; Geng, B.; Zhang, Q. *Inorg. Chem.* **2014**, *53*, 8529−8537.
(17) Xiong, W.-W.; Li, P. Z.; Zhou, T. H.; Tok, A. I. Y.; Xu, R.; Zhao, Y.; Zhang, Q. *Inorg. Chem.* **2013**, *52*, 4148−4150.
(18) Sheldrick, G. M. *SHELX-97*; Universität Göttingen: Germany, 1997.
(19) Wang, Z.; Xu, G.; Bi, Y.; Wang, C. *CrystEngComm* **2010**, *12*, 3703−3707.
(20) (a) Browne, A. W.; Shetterly, F. F. *J. Am. Chem. Soc.* **1908**, *30*, 221−237. (b) Welsh, T. W. B.; Broderson, H. J. *J. Am. Chem. Soc.* **1915**, *37*, 816−824. (c) Kirk, R. E.; Browne, A. W. *J. Am. Chem. Soc.* **1928**, *50*, 337−347.
(21) (a) Block, E.; Ofori-Okai, G. *J. Am. Chem. Soc.* **1992**, *114*, 758−759. (b) Schrauzer, G. N.; Kiefer, G. W.; Tano, K.; Doemeny, P. A. *J. Am. Chem. Soc.* **1974**, *96*, 641−652. (c) Schrock, R. R.; Glassman, T. E.; Vale, M. G. *J. Am. Chem. Soc.* **1991**, *113*, 725−726.
(22) Liu, Y.; Kanhere, P. D.; Ling Wong, C.; Tian, Y.; Feng, Y.; Boey, F.; Wu, T.; Chen, H.; White, T. J.; Chen, Z.; Zhang, Q. *J. Solid State Chem.* **2010**, *183*, 2644−2649.
(23) Liu, Y.; Tian, Y.; Wei, F.; Ping, M. S. C.; Huang, C.; Boey, F.; Kloc, C.; Chen, L.; Wu, T.; Zhang, Q. *Inorg. Chem. Commun.* **2011**, *14*, 884−888.
(24) Schaefer, M.; Näther, C.; Bensch, W. *Solid. State Sci.* **2003**, *5*, 1135−1139.
(25) Gao, J. K.; Tay, Q. L.; Li, P. Z.; Xiong, W. W.; Zhao, Y. L.; Chen, Z.; Zhang, Q. *Chem. Asian J.* **2014**, *9*, 131−134.
(26) (a) Mitzi, D. B. *Inorg. Chem.* **2005**, *44*, 3755−3761. (b) Mitzi, D. B. *Inorg. Chem.* **2007**, *46*, 926−931.
(27) (a) Ahari, H.; Garcia, A.; Kirkby, S.; A. Ozin, G.; Young, D.; J. Lough, A. *Dalton Trans.* **1998**, *37*, 2023−2028. (b) Zhang, Q.; Bu, X.; Han, L.; Feng, P. *Inorg. Chem.* **2006**, *45*, 6684−6687. (c) Van Almsick, T.; Sheldrick, W. S. *Acta Crystallogr.* **2005**, *E61*, m2348−m2350.
(28) van Almsick, T.; Loose, A.; Sheldrick, W. S. *Anorg. Allg. Chem.* **2005**, *631*, 21−23.
(29) Kromm, A.; Sheldrick, W. S. *Z. Anorg. Allg. Chem.* **2008**, *634*, 1005−1010.
(30) Haddadpour, S.; Niedermeyer, H.; Clerac, R.; Dehnen, S. *Dalton Trans.* **2009**, *38*, 8162−8164.
(31) (a) Brandmayer, M. K.; Clerac, R.; Weigend, F.; Dehnen, S. *Chem.—Eur. J.* **2004**, *10*, 5147−5157. (b) Thiele, G.; Peter, S.; Schwarzer, M.; Ruzin, E.; Clerac, R.; Staesche, H.; Rosser, C.; Roling, B.; Dehnen, S. *Inorg. Chem.* **2012**, *51*, 3349−3351. (c) Dhingra, S. S.; Haushalter, R. C. *Chem. Mater.* **1994**, *6*, 2376−2381.
(32) Pienack, N.; M?ller, K.; Nather, C.; Bensch, W. *Solid State Sci.* **2007**, *9*, 1110−1114.
(33) Philippidis, A.; Trikalitis, P. N. *Polyhedron* **2009**, *28*, 3193−3198.
(34) Xiong, W. W.; Li, P. Z.; Zhou, T. H.; Zhao, Y.; Xu, R.; Zhang, Q. *J. Solid State Chem.* **2013**, *204*, 86−90.
(35) (a) Bhanage, B. M.; Fujita, S.; Ikushima, Y.; Arai, M. *Green Chem.* **2003**, *5*, 340−342. (b) Wu, C. Y.; Cheng, H. Y.; Liu, R. X.; Wang, Q.; Hao, Y. F.; Yu, Y. C.; Zhao, F. Y. *Green Chem.* **2010**, *12*, 1811−1816. (c) Tamura, M.; Noro, K.; Honda, M.; Nakagawa, Y.; Tomishige, K. *Green Chem.* **2013**, *15*, 1567−1577.
(36) Axtell, E. A.; Hanko, J.; Cowen, J. A.; Kanatzidia, M. G. *Chem. Mater.* **2001**, *13*, 2850−2863.